J Nanopart Res (2009) 11:1957–1969
DOI 10.1007/s11051-008-9554-1

RESEARCH PAPER

Neurotoxicity of manganese oxide nanomaterials

Diana M. Stefanescu · Ali Khoshnan · Paul H. Patterson · Janet G. Hering

Received: 1 March 2008 / Accepted: 25 October 2008 / Published online: 19 November 2008

Abstract Manganese (Mn) toxicity in humans has been observed as manganism, a disease that resembles Parkinson's disease. The mechanism of Mn toxicity and the chemical forms that may be responsible for its neurotoxicity are not well understood. We examined the toxicity of Mn oxide nanomaterials in a neuronal precursor cell model, using the MTS assay to evaluate mitochondrial function in living cells and the LDH assay to quantify the release of the enzyme lactate dehydrogenase as a result of damage to the cell membrane. Both assays show that the toxicity of Mn is dependent on the type of Mn oxide nanomaterial and its concentration as well as on the state of cell differentiation. Following exposure to Mn oxide nanomaterials, reactive oxygen species (ROS) are generated, and flow cytometry experiments suggest that cell death occurred through apoptosis. During exposure to Mn oxide nanomaterials, increased levels of the transcription factor NF-κB (which mediates the cellular inflammatory response) were observed.

Keywords Nano · Manganese oxide · Toxicity · Neurons · Manganism · Parkinson's disease · Nanoparticles · Nanomedicine

D. M. Stefanescu · J. G. Hering
Department of Environmental Science and Engineering, 138-78, California Institute of Technology, Pasadena, CA 91125, USA

Present Address:
D. M. Stefanescu
Air Liquide, Delaware Research and Technology Center, 200 GBC Dr., Newark, DE 19702, USA

A. Khoshnan · P. H. Patterson (✉)
Division of Biology, 216-76, California Institute of Technology, Pasadena, CA 91125, USA
e-mail: php@caltech.edu

Present Address:
J. G. Hering
Swiss Federal Institute of Aquatic Science and Technology, Überlandstrasse 133, 8600 Dübendorf, Switzerland

Introduction

The current and potential industrial applications of nanomaterials have been widely publicized, but concerns about their health and environmental safety have only recently received attention. Interest in nanotoxicity is motivated by the rapidly expanding manufacture and use of nanomaterials and by the recognition that the health impacts of nanoparticles (NP's) may be more severe than that of the corresponding bulk materials (Colvin 2003). A recent review by Nel et al. (2006) highlighted the concern that NP's may affect biological processes at cellular, sub-cellular, and protein levels and that such effects may be exacerbated by the mobility of some NP's within the body. With decreasing size, the ratio between mass and surface area increases rapidly (Kreyling et al. 2006; Oberdorster 2001). Thus, higher reactivity and toxicity are expected for NP's

compared to their bulk equivalents (Colvin 2003). As a result of their specific surface area, nanomaterials can be biologically active even if the bulk material is inert (Goodman et al. 2004). A wide variety of chemical elements have already been incorporated into NP's and more are anticipated to be used for such applications in the near future. Current NP applications range from burn and wound dressing to sunscreens and cosmetics, fuel cells, tires, optics, clothing, and electronics (Oberdorster et al. 2005). Literature documents the toxicity associated with exposure to ultrafine particles through inhalation (Oberdorster 2001). Translocation of particles is dependent on particle size, and NP's of varying compositions preferentially target mitochondria (Oberdorster et al. 2005).

Therefore, an assessment and identification of the possible hazards related to the release of nanomaterials into the environment is needed. Such an investigation requires a study of toxicity in appropriate cell and animal models as well as analysis of nanoparticle size, shape, composition, and solubility. Mn-containing nanomaterials provide a useful test case for nanotoxicity studies because of the known neurotoxicity (Dobson et al. 2004) associated with Mn exposure. The occupational disease of manganism in its later stages resembles Parkinson's disease (Fechter et al. 2002). Upon inhalation, both soluble and insoluble forms of Mn are known to be translocated along the olfactory nerve and across the blood–brain barrier (Brenneman et al. 2000). The mechanism of uptake and transport of metals into the olfactory system was studied for particles containing Mn, cadmium, nickel, mercury, or iron (Tjalve and Henriksson 1999; Rao et al. 2003), but only Mn was found to be taken up preferentially via the olfactory pathway. Moreover, the absorption of Mn in the lung appears to be dependent on particle solubility and size (Dorman et al. 2001; Elder et al. 2006), but dissolution is not a pre-requisite for neuronal uptake and transportation to the brain. Dissolved Mn can be found in nature at very low concentrations only ($\sim 2 \times 10^{-7}$ in rivers) and Mn oxides are known to be particularly insoluble (Morgan 2000). Elder et al. (2006) analyzed the solubility of Mn oxide ultrafine particles and found that at room temperature, the particles dissolved at a rate of 1–1.5% per day at a neutral pH. However, acidification to pH = 4.5 resulted in a rapid dissolution.

Sources of ultrafine Mn oxide particles include ferroalloy production, iron and steel foundries and power plant and coke oven combustion emissions (Vitarella et al. 2000). In addition, the organic Mn compound methylcyclopentadienyl manganese tricarbonyl (MMT), is presently used as antiknock agent in gasoline primarily in Canada and Australia (Gulson et al. 2006; Cohen et al. 2005) and the combustion of fuels amended with MMT could release Mn-containing particles into the atmosphere. In all of these cases, the most likely route of human exposure would be through inhalation.

In this study, we synthesized insoluble Mn oxide nanomaterials of various sizes and compositions. We then examined their uptake in rat ST-14 cells, a neuronal precursor cell model, and the corresponding nondividing post-mitotic neurons (differentiated from ST-14 cells) and assessed the effects of particle size and composition. The mechanisms of toxicity and cell death were also studied.

Experimental section

Synthesis of nanomaterials

$Mn(II,II)_3O_4$ NP's were prepared by heating $KMnO_4$ in a mixture of 45 mL of 60% ethanol and 40% water at 160 °C for 8 h in a 125 mL autoclave. A brown slurry was formed. The NP's were centrifuged, then washed twice with water, and then dried in a vacuum oven at 55 °C overnight. The size of the NP's was dependent on the amount of $KMnO_4$ used in the reaction. For small, medium, and large NP's, the amount of $KMnO_4$ was 0.25, 0.5, and 1 g, respectively. Mn(III)OOH was prepared by heating 0.5 g of $KMnO_4$ in a 45 mL mixture of 2.9% ethanol and 97.1% water in a 125 mL autoclave at 140 °C for 15 h. $K_xMn(IV)O_2$ was prepared by decomposition of 0.18 g of $KMnO_4$ in 6.5 mL of water at 160 °C for 8 h in a 45 mL autoclave. The materials were further centrifuged, then washed twice with water, and then dried in a vacuum oven at 55 °C.

Characterization of nanomaterials

Transmission Electron Microscopy (TEM)

Transmission Electron Microscopy was done on a Philips EM420 microscope at 120 kV. The samples were prepared by suspending the solid powder in

H_2O using sonication ($c = 1$ mg/mL) and then the suspension was deposited on carbon coated Cu grids. Size measurements were done using J-Image software (available at http://rsb.info.nih.gov/ij/).

BET

Surface area measurements were performed on a Gemini 2360 BET analyzer.

XRD

Powder X-ray Diffraction analysis was performed with an X'Pert Philips diffractometer using a Cu K_α radiation (1.541874 Å). The XRD pattern for Mn_3O_4 NP's can be indexed to the tetragonal Mn_3O_4 (JCPDS 24-0734) and the one for MnOOH nanotubes can be indexed to MnOOH (JCPDS 41-1379). K_xMnO_2 synthesis produced an amorphous material.

Cell culture

ST-14 rat striatal neuroblasts were grown at 33 °C in DMEM (Dubelcco's Modified Eagle's Medium), supplemented with 10% Fetal Bovine Serum, penicillin (100 IU/mL), streptomycin (100 μg/mL), and 2 mM L-glutamine in a 95% air–5% CO_2 humidified incubator. Differentiated neurons were grown from ST-14 rat striatal neuroblasts at 39 °C in DMEM containing F12 Nutrient, N_2 supplement, penicillin (100 IU/mL), streptomycin (100 μg/mL), and 2 mM L-glutamine in a 95% air–5% CO_2 humidified incubator for 5 days.

Cytotoxicity assays

Cells were grown to 60–70% confluency and then incubated with the corresponding nanomaterial. Before being added to the cells, the nanomaterials were sonicated in water at a concentration of 1 mg/mL, and then diluted in the cell medium up to the desired concentration (1, 2.5, 5, and 10 μg/mL). After 48 h, the cells were used for mitochondrial activity evaluation (MTS assay), while the supernatant for the lactate dehydrogenase (LDH) assay. For the MTS assay, CellTiter 96 aqueous nonradioactive assay (Promega) was used. The cells were washed twice with DMEM and then 20 μL of MTS reagent were added into 100 μL fresh medium and then further incubated. After 1–2 h, absorbance at 490 nm was measured. The color intensity is direct proportional to the mitochondrial activity of the cells, an indirect evidence for cell viability. The relative cell viability (%) related to control wells containing cell culture medium only was calculated using $A_{test}/A_{control} * 100$. A_{test} and $A_{control}$ are the average absorbance of the test sample and control. For LDH leakage, CytoTox 96® NonRadioactive Cytotoxicity Assay (Promega) was used. The LDH released in culture supernatants is measured with a 30-min coupled enzymatic assay. The amount of color formed is proportional to the number of lysed cells.

For the assay on differentiated neurons, cells were grown to confluency in 24-well plates and then differentiated for 5 days into neurons according to published procedures (Böttcher et al. 2003).

After 48 h from nanomaterial addition, the LDH containing medium was collected and 50 μL of each sample was plated in a 96-well plate in triplicate. Next, 50 μL of substrate solution was added to the wells, and plates were incubated for 30 min at room temperature. The relative LDH leakage (%) related to control wells containing cell culture medium only was calculated using $A_{test}/(A_{control} + A_{lysed}) * 100$. A_{test} and $A_{control}$ are average absorbances from the spontaneous LDH release of the tested sample and control in the medium, and A_{lysed} is the absorbance from the intentionally lysed cells of the control sample.

For both assays, absorbance was measured with a Spectra Max 190 microplate reader from Molecular Devices. The spectrometer was calibrated to zero absorbance using culture medium without cells.

TEM on cells

ST-14 cells and differentiated neurons were treated separately with small NP and K_xMnO_2 ($c = 10$ μg/mL) for 48 h. Cells were then harvested and processed into polymerized blocks, which were sectioned at 500–700 nm thickness and examined with a Philips EM 210 microscope. Processing was done according to already published procedures (Phillips 1998).

ROS measurements

DCF assay

ST-14 cells (25,000) were seeded in 96-well plates. After 48 h, the cells were washed in Hank's balanced

salt solution (HBSS) then incubated with 2′7′-dichlorodihydrofluorescein (H_2DCFDA, 2.5 μM), Molecular Probes at 37 °C. H_2DCFDA is a cell-permeant indicator for ROS that is nonfluorescent until the acetate groups are removed by intracellular esterases and oxidation occurs within the cell. The cells were then washed twice with HBSS, incubated with Mn nanomaterials Mn_3O_4, MnOOH, or K_xMnO_2 at concentrations of 1, 2.5, 5, and 10 μg/mL. Fluorescence measurements were performed immediately and after 1 h of treatment using a fluorescence plate reader FLx 800 microplate fluorescence reader from Bio-tek Instruments at 485 nm excitation and 530 nm emission wavelengths. Cells not treated with nanomaterials were used as control.

Statistical analysis

Results are presented as mean ± standard deviation. The data were analyzed for statistical difference using student *t*-test. Statistical significance was accepted at a level of $p < 0.05$.

Gene reporter assays

ST-14 alfa cells are grown in 6-well plates over 24 h and transfected in presence of lipofectamine (Lipofectamine Reagent 2000 from Invitrogen) with NF-κB or p53 gene reporter plasmid fused to luciferase and with the gene promoters plasmids beta-gal (for normalization) and ε-GFP (for transfection control). After 24 h, the medium containing the transfection reagent was removed, and cells were treated with the corresponding nanomaterials. The cells were harvested at 6, 12, 16, 20, and 24 h after nanomaterial addition. Nontreated cells are used as control and are harvested at 24 h. Some experiments were done up to 48 h. Cells were then lysed in reporter lysis buffer (150 μL for three wells) for 10 min on ice, then centrifuged at 4 °C for 2 min and the lysate was used for luciferase and beta-gal assays.

Luciferase assay

For measuring the NF-κB or p53 activation upon NP's addition, a luciferase assay (Promega) was used. In this assay, firefly luciferase catalyzes luciferin oxidation forming the product molecule oxyluciferin. In the process, light is emitted and its intensity is measured. A total of 20 μL of cell lysate was combined with 100 μL of luciferin substrate, and then the light intensity is measured with a Monolight 2010 luminometer from Analytical Luminescence Laboratory for 10 s. The measurements were done in triplicate and then averaged. The light intensity is directly proportional to NF-κB activity.

Beta-gal assay

Beta-gal assay is used for measuring the levels of active beta-galactosidase expressed in transfection. Measuring the beta-galactosidase levels assists with the normalization of the NF-κB activation. In this assay, beta-galactosidase catalyzes the hydrolysis of beta-galactosides such as ortho-nitrophenyl-D-galactopyranoside (ONPG) to the ONP anion producing a bright yellow color with a peak absorbance at 420 nm. A total of 50 μL of cleavage buffer were plated with 17 μL of ONPG and 15 μL of cell lysate in 96-well plates and then incubated for 30 min at 37 °C. Absorbance at 420 nm was measured with a Spectra Max 190 microplate reader from Molecular Devices. The spectrometer was calibrated to zero absorbance using cleavage buffer and ONPG as blank. The color intensity is directly proportional to the beta-galactoside activity. Measurements were done in triplicate for each condition and averaged.

Normalization of NF-κB activity

The absorbance measured with the beta-gal assay of the tested sample is divided by the absorbance of the control $r = A_{test}/A_{control}$. Then the light intensity (l.i.) from the luminometer is divided by the absorbance ratio l.i./r.

Flow cytometry experiments for cell apoptosis quantification

ST-14 cells were treated with small Mn_3O_4 NP at concentrations of 0, 2.5, 5, and 10 μg/mL for 36 h. Apoptotic cells were distinguished from necrotic cells using Invitrogen's Vybrant Apoptosis Kit #2 (Carlsbad CA) and assayed by flow cytometry. Cells were run on a BD Biosciences FACSCalibur flow cytometer equipped with an air-cooled Argon 488 nm laser. Essentially, the apoptotic cells were labeled with 4 μl/10^6 cells Alexa Fluor 488 conjugated annexin-V

(emitting green fluorescence in FL1-530 nm) and necrotic cells were labeled with 1.5 μg/10^6 cells of the nucleic acid binding dye Propidium Iodide (PI) (emitting red fluorescence in FL2-575 nm) in 1× annexin-binding buffer. Live cells have intact cell surface membranes which exclude PI staining. Apoptotic cells, on the other hand, lose their membrane asymmetry and translocate their phosphatidylserine from the inner to the outer surface of their plasma membrane, which then highly bind the annexin-V Alexa Fluor 488 conjugate and also exhibit low to medium PI fluorescence. Dead cells show both high annexin-V-Alexa Fluor 488 binding and high PI fluorescence.

Results and discussion

Synthesis and characterization of nanomaterials

Published procedures were followed (with minor modifications as described in the "Experimental section"), to synthesize Mn_3O_4, MnOOH, and K_xMnO_2 nanomaterials (Zhang et al. 1999, 2004). These were synthesized from $KMnO_4$ in water in the presence of ethanol to obtain Mn_3O_4 (Scheme 1) and MnOOH and without ethanol to obtain K_xMnO_2. For Mn_3O_4 nanoparticles (NP's), the $KMnO_4$ concentration range for obtaining NP's has been previously published, but no correlation between the concentration of $KMnO_4$ used in the synthesis and Mn_3O_4 particle size was made. We found that lower concentrations of the $KMnO_4$ reagent starting material lead to smaller NP sizes.

As shown by TEM (Fig. 1), Mn_3O_4 NP's were obtained in three size classes with diameters of 70–120 (s), 150–220 (m), and 200–350 (l) nm.

The diameters of the MnOOH nanotubes ranged from 200 to 400 nm and those of the K_xMnO_2 nanofibers from 5 to 10 nm. Both nanotubes and

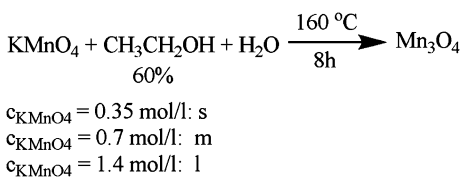

Scheme 1 Conditions for the synthesis of small (s), medium (m), and large (l) Mn_3O_4 NP's

fibers had lengths of a few μm, but their individual length was difficult to quantify due to their high agglomeration. Mineralogy was confirmed by X-ray diffraction and was consistent with previous reports. The UV–vis absorbance spectra of the Mn_3O_4 NP's exhibits shifts toward higher wavelengths with increasing size. Specific surface areas (m^2/g) determined by BET (Brunauer–Emmet–Teller method) were 11.2–15.7 (s), 6.9–7.8 (m), 5.9–8.5 (l) for Mn_3O_4, 32.5–46.8 for MnOOH, and 102.8–137.5 for K_xMnO_2.

Cytotoxicity of nanomaterials

Cytotoxicity studies of Mn nanomaterials were performed on dividing ST-14 rat striatal neuroblasts and nondividing post-mitotic neurons (differentiated from ST-14 cells) using two colorimetric assays. The MTS assay is used to evaluate the mitochondrial activity in living cells and the LDH assay is used to evaluate cell damage, from the release of the enzyme lactate dehydrogenase into the cell medium. Mitochondrial activity and/or enzyme leakage were assayed after exposure of (dividing) ST-14 neuroblasts and of differentiated (nondividing) neurons to the Mn oxide nanomaterials at various concentrations for 48 h. In both cytotoxicity assays, the small Mn_3O_4 NP's exert the strongest cytotoxicity. The effect of small Mn_3O_4 on mitochondrial activity increases linearly with concentration (Fig. 2); however, only a modest effect of concentration is observed for medium or large Mn_3O_4, MnOOH, or K_xMnO_2.

In the LDH assay, the proportion of lactate dehydrogenase found in the cell medium (relative to the value obtained from control cells) increases with NP concentration for medium and large Mn_3O_4 NP's. For small NP's, the proportion of lysed cells appears to reach a plateau at a NP concentration between 2.5 and 5 μg/mL (Fig. 3). At the highest concentration tested (10 μg/mL), K_xMnO_2 produced the least enzyme leakage, followed by MnOOH.

Both MTS and LDH assays were attempted after treating the cells with nanomaterials for 24 h only, but no significant toxicity was observed except for small Mn_3O_4 nanoparticles.

For differentiated neurons, treatment for 48 h with Mn_3O_4, MnOOH, or K_xMnO_2 causes significant cell damage only at 10 μg/mL (data not shown). Thus, the nondividing differentiated neurons are less sensitive

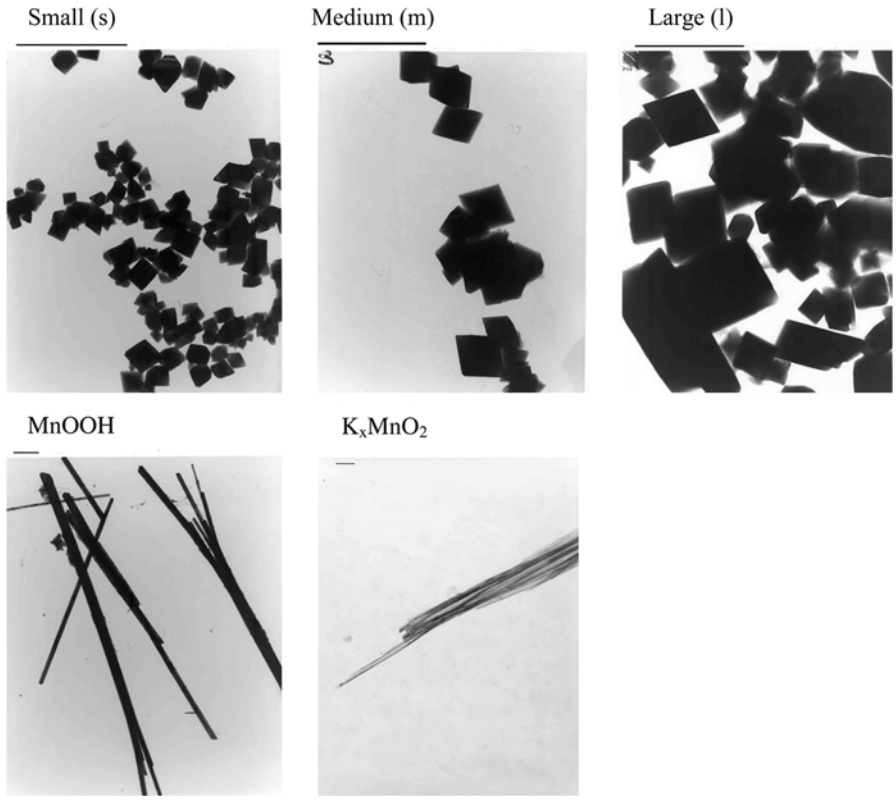

Fig. 1 Transmission Electron Microscopy images of nanomaterials illustrate the variety of shapes and sizes that are obtained. The scale bar is 1 μm for Mn_3O_4 and MnOOH and 100 nm for K_xMnO_2

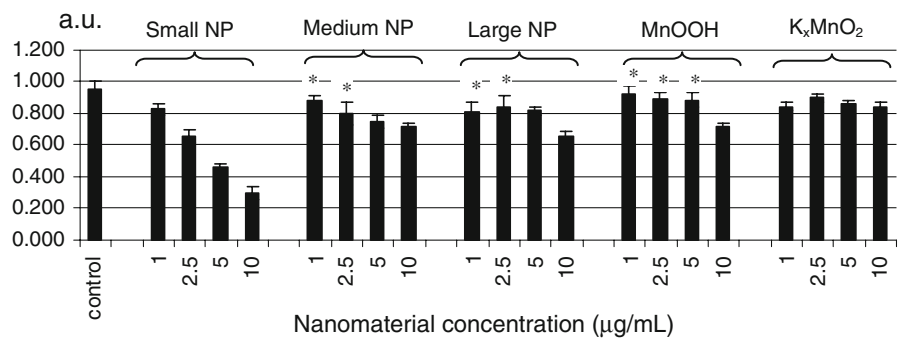

Fig. 2 Results of the MTS assay of mitochondrial activity of the dividing ST-14 cells exposed to small (s), medium (m), or large (l) Mn_3O_4, MnOOH, and K_xMnO_2 as a function of concentration (in μg/mL) of the nanomaterials. The MTS assay quantifies the enzymatic conversion of a tetrazolinium salt (MTS) into a soluble brown formazan product by mitochondrial dehydrogenase. The absorbance (a.u. = absorbance units) of the colored product is measured. The "control" result was obtained with cells not exposed to nanomaterials. "*" = values are not statistically different from the control

to the Mn nanomaterials than the dividing cells, which exhibited cell damage at lower nanomaterial concentration, particularly for Mn_3O_4.

These results are in agreement with previous findings showing that (a) NP toxicity is concentration dependent, even in the absence of toxicity of the corresponding soluble salt, (b) effects on cell morphology, mitochondrial function and apoptosis are dependent on both nanoparticle composition and concentration, and, (c) the same type of NP's can show differential toxicity on diverse cell lines (Braydich-Stolle et al. 2005; Brunner et al. 2006). For instance the effects of 15 nm Ag, 30 nm MoO_3, and 30 nm Al NP's have been examined at concentrations of 5–100 μg/mL on mammalian germline stem cells and it was observed that cell morphology,

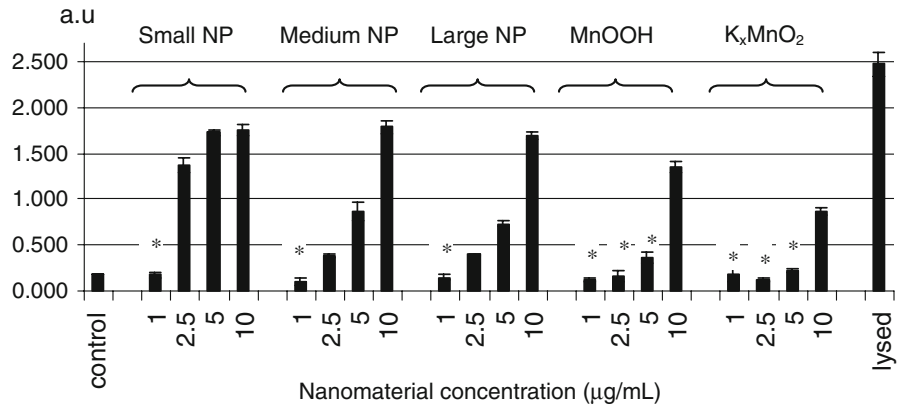

Fig. 3 Results of the LDH assay of cell damage in dividing ST-14 cells exposed to small (s), medium (m), or large (l) Mn_3O_4, MnOOH, and K_xMnO_2 as a function of concentration (in μg/mL) of the nanomaterials. The LDH assay quantifies the conversion of a tetrazolinium salt (INT) into a soluble formazan product by means of lactate dehydrogenase, an enzyme which is released into the culture supernatant upon cell damage and is subsequently stable. The absorbance (a.u. = absorbance units) of the colored product is measured. The "control" result was obtained with cells not exposed to nanomaterials. The "lysed" result was obtained upon intentional lysis of the control cells. "*" = values were not statistically different from the control

mitochondrial function, and apoptosis are dependent on both NP composition and concentration (Braydich-Stolle et al. 2005). Similar studies of the toxicity of Ag, Al, MoO_3, Fe_3O_4, and TiO_2 NP's reported severe toxicity of Ag NP's and moderate toxicity of MoO_3 NP's on rat liver derived cell line (BRL 3A) (Hussain et al. 2005). The cytotoxicity of Ag (15 and 100 nm) in liver cells is likely to be mediated through oxidative stress, while the microscopic studies demonstrated that cells exposed to NP's at higher doses became abnormal in size, displaying cellular shrinkage, and an acquisition of an irregular shape.

Brunner et al. (2006) studied the toxicity of several NP's (CeO_2, ZrO_2, Fe_2O_3, ZnO, $Ca_3(PO_4)_2$, and TiO_2) on Mesothelioma cells MSTO-211H and 3T3 Swiss Albino mouse fibroblasts. In the case of zinc oxide (ZnO) all MSTO or 3T3 cells died after exposure to ZnO NP concentrations above 15 ppm. Treatment of cell cultures with nanoparticulate uncoated iron oxide (Fe_2O_3) revealed a cell-type specific response. Slower proliferating 3T3 cells were only slightly affected by addition of up to 30 ppm iron oxide, while the cell parameters (MTT-conversion and DNA content) of the faster growing MSTO cells were drastically reduced upon exposure to only 3.75 ppm iron oxide. After exposure to ceria, titania, or zirconia, cell cultures showed a comparable response after 3 days where the values of the cell parameters were affected with increasing concentration. MSTO cells exhibited a higher sensitivity to the NP's than 3T3 cells.

Size-dependent studies of Au NP's on four different cell lines: HeLa cervix carcinoma epithelial cells, SK-Mel-28 melanoma cells, L929 mouse fibroblasts, and mouse monocytic/macrophage cells (J774A1) and it was shown that 1.4 nm Au NP's show higher cytotoxicity than 15 nm NP's (Pan et al. 2007) independent of the cell line tested.

Mechanism of cytotoxicity and cell death

We explored possible mechanisms of the cytotoxicity effects of nanomaterials using TEM to locate the NP's within the ST-14 cells and neurons, measuring the production of reactive oxygen species (ROS), the activation of the transcription factor NF-κB as well as apoptosis.

Cells and differentiated neurons were treated with small NP's or K_xMnO_2. Following incubation for 48 h, cells were processed using standard procedures (Phillips 1998) into polymerized blocks, which were sectioned and examined by TEM. Both particles and fibers are taken up and found in the cytoplasm (Fig. 4), without apparently penetrating into the nucleus.

In Fig. 4, aggregates of the nanomaterials are clearly visible within the cells/neurons. It is not known, however, whether this aggregation occurred

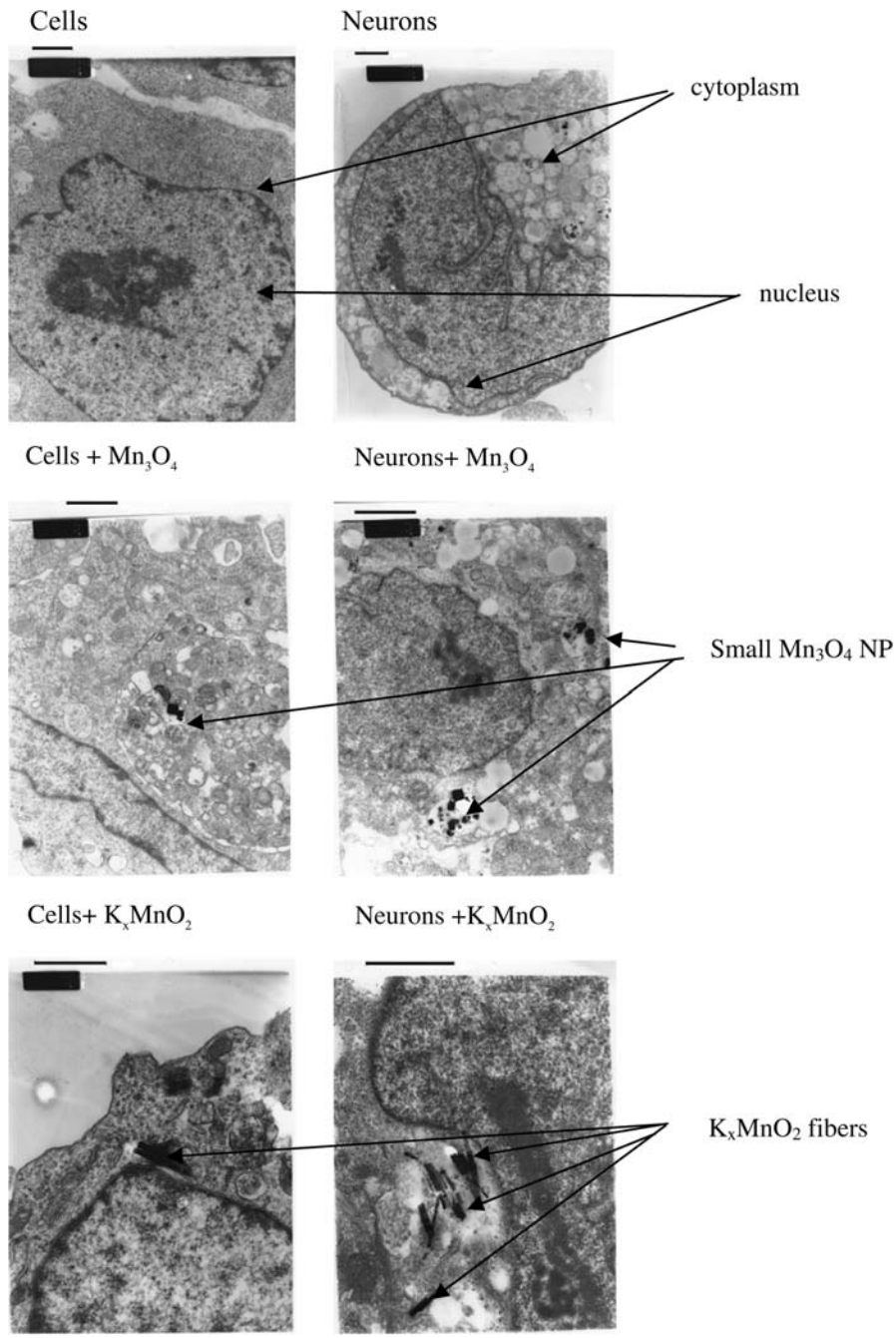

Fig. 4 Transmission electron microscopy of cells and neurons treated with small Mn_3O_4 NP's or K_xMnO_2. Scale = 1 μm

within the cells/neurons or in the external media. The extent of aggregation in the external media would be expected to vary depending on the composition of the media and to affect the uptake of the nanomaterials. With regard to aggregation, one potentially important difference between the media used for dividing cells and differentiated neurons is that only the cell growth medium contains the protein supplement fetal bovine serum. The protein ovalbumin has been used as a surfactant to stabilize NP's of hydroxyapatite (Zhao et al. 2008) and iron oxide particles have been embedded in microspheres of human serum albumin (Chatterjee et al. 2001). Although some interaction between the proteins and Mn oxide nanomaterials in our system may be expected, it is difficult to predict the influences on aggregation behavior.

These results are consistent with other recent studies on cells treated with NP's like PVC (polyvinyl chloride), TiO_2, SiO_2, Co, Ni, or Au or quantum dots of various sizes. NP's penetrate into the cell leading to mitochondrial damage and apoptosis (Xia et al. 2006; Chithrani and Chan 2007; Long et al. 2006; Peters et al. 2004; Rahman et al. 2002; Li et al. 2003). A possible mechanism would be NP uptake through endocytosis (Chang et al. 2006; Chithrani and Chan 2007). According to Chithrani and Chan (2007), NP's penetrate most easily through the cell membrane when their size is $\leq$55 nm (a single particle or an aggregate of smaller particles). NP's $>$ 55 nm are taken up into the cells, but at a slower rate.

Oxidative stress and the generation of ROS are key mechanisms in cellular defense after particle uptake (Churg 2003). Reactive oxygen species are reported to be the main source of toxicity associated with environmental NP's (diesel exhaust particles; DEP) (Hiura et al. 1999; Kumagai et al. 2002; Li et al. 2000), as well as with some engineered nanomaterials (single-walled carbon nanotubes, silver NP's, etc.) (Brunner et al. 2006; Xia et al. 2006; Long et al. 2006; Li et al. 2003; Manna et al. 2005; Limbach et al. 2007).

Exposure to Mn has been associated with glial activation, ROS production and secretion of pro-inflammatory cytokines (Filipov et al. 2005; Hiura et al. 1999). We studied ROS production in the ST-14 cells following treatment with Mn oxide nanomaterials (Fig. 5).

Significant ROS production was observed for all Mn nanomaterials. ROS formation was greatest in cells exposed to K_xMnO_2, followed by MnOOH and small Mn_3O_4 NP's. Medium and large Mn_3O_4 NP's showed the smallest amount of ROS formation.

Limbach et al. (2007) recently investigated ROS formation upon addition of iron, cobalt, titania, or manganese oxides NP's to lung epithelial cells. These NP's have similar morphology, size, shape, and degree of aggregation. It was shown that Mn_3O_4 NP's generated the highest ROS levels, followed by Co_3O_4, Fe_2O_3, and TiO_2 in decreasing order.

The presence of oxidative stress can cause the induction of cytokines [e.g., Tumor Necrosis Factor-α (TNF-α)] or DNA damage, potentially leading to the activation of the transcription factors NF-κB and p53, respectively. NF-κB regulates expression of hundreds

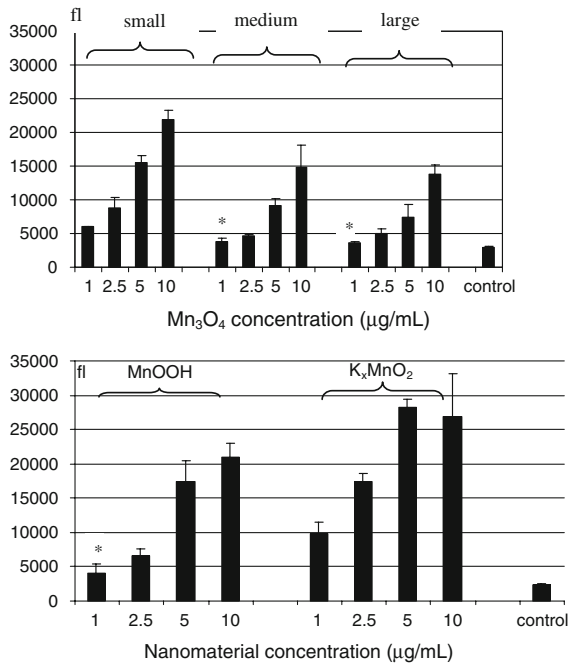

Fig. 5 Fluorescence (fl) generated by intracellular oxidation of an indicator for reactive oxygen species formation is examined in dividing ST-14 cells treated with Mn_3O_4, MnOOH, or K_xMnO_2 for 1 h at concentrations of 1, 2.5, 5, and 10 μg/mL. Cells were incubated with the nonfluorescent form of the indicator before exposure to the nanomaterials. The "control" result was obtained with cells not exposed to nanomaterials. "*" = values were not statistically different than the control

of genes that are implicated in cell survival, apoptosis, inflammation cancer, and metastasis and promotes expression of pro-survival genes in response to ROS by blocking programmed cell death (Sakon et al. 2003; Pahl 1999). Aberrant regulation of NF-κB has been linked to cancer, inflammatory and autoimmune diseases, viral infection, and neuronal death. The transcription factor p53 can activate DNA repair proteins when DNA is damaged and can initiate apoptosis if the DNA damage proves irreparable. Since it was previously shown that DEP and single-walled carbon nanotubes activate the NF-κB pathway (Takizawa et al. 1999), we investigated the effect of Mn_3O_4 NP's on NF-κB and p53 activation. No significant increase in p53 activity on treatment with NP's over 48 h is observed, while NF-κB activation is concentration dependent.

ST-14 cells were transfected with an NF-κB-luciferase reporter plasmid, then treated with small NP's (c = 2.5, 5, 10 μg/mL). The results show that

NP's increase NF-κB activity in a concentration-dependent manner (Fig. 6). A maximum increase at 12 and 16 h is observed at 10 μg/mL, which is followed by a decrease that is likely due to cell death. The effect of NP's on NF-κB activation was less pronounced at 5 μg/mL, and no effect (relative to control) was observed at 2.5 μg/mL.

Oxidative stress can cause subsequent cell death by apoptosis or necrosis. Apoptosis, or programmed cell death is executed in such a way as to safely dispose of cell fragments. Necrosis involves accidental death of cells and living tissue, which hinders the removal of cell debris by phagocytosis. ST-14 cells were treated with the small Mn_3O_4 NP's at several concentrations for 36 h and apoptotic cells were distinguished from necrotic cells by means of flow cytometry. An increase in apoptotic cells was observed with increasing NP concentration, while the fraction of dead cells remains the same (Fig. 7). This suggests that upon addition of NP's, cell death occurs through apoptosis up to a NP concentration of 10 μg/mL. About 3.6% of the cells undergo early apoptosis, in the absence of Mn_3O_4 NP's, while the percentage increases to 9.7, 19.2, and 36.4 for the cells treated with 2.5, 5, or 10 μg/mL small Mn_3O_4 NP's, respectively.

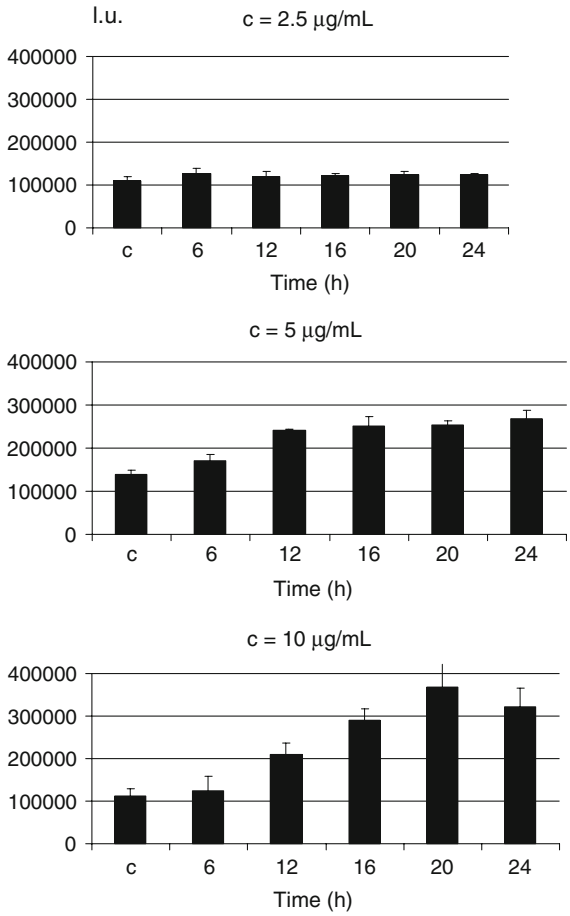

Fig. 6 Activation of NF-κB determined from the luciferase assay (l.u. = luminescence units) normalized using the beta-gal assay as described in the "Experimental section." Results are shown for ST-14 cells exposed to varying concentration of small Mn_3O_4 NP's as a function of the exposure time and for unexposed cells (control)

Similar experiments have been performed with DEP and other engineered NP's. It was shown that DEPs induce apoptosis in macrophages (Li et al. 2003; Hiura et al. 2000) while upon treatment with cadmium oxide or molybdenum NP's, mammalian germline stem cells undergo death by apoptosis at low NP concentration, while at higher concentrations, more cells become necrotic (Braydich-Stolle et al. 2005).

Conclusions

In summary, we synthesized three different Mn oxide nanomaterials, Mn_3O_4 NP's, MnOOH nanotubes, and K_xMnO_2 nanofibers. In addition, three size classes (small, medium, and large) of the Mn_3O_4 NP's were synthesized. The synthesized nanomaterials differed substantially in their specific surface area, which decreased in the order $K_xMnO_2 \gg$ MnOOH $\gg$ small Mn_3O_4 > medium Mn_3O_4 > large Mn_3O_4.

The cytotoxicity of the nanomaterials was assessed on the basis of the inhibition of mitochondrial activity (MTS assay) and cell damage (LDH assay). With both assays, the most pronounced effects were observed with small Mn_3O_4 followed by medium and large Mn_3O_4; a distinct concentration dependence was observed in the MTS assay for small Mn_3O_4 and for all Mn_3O_4 NP's in the LDH assay. With MnOOH and K_xMnO_2, comparable effects were observed on mitochondrial activity and slightly more cell damage with MnOOH than with K_xMnO_2; a weak concentration dependence was observed only in the LDH assay. In general, stronger cytotoxic effects were observed with dividing ST-14 cells than with differentiated neurons. TEM studies showed that Mn_3O_4 and K_xMnO_2 nanomaterials were taken up by both dividing cells and neurons, but appeared to be

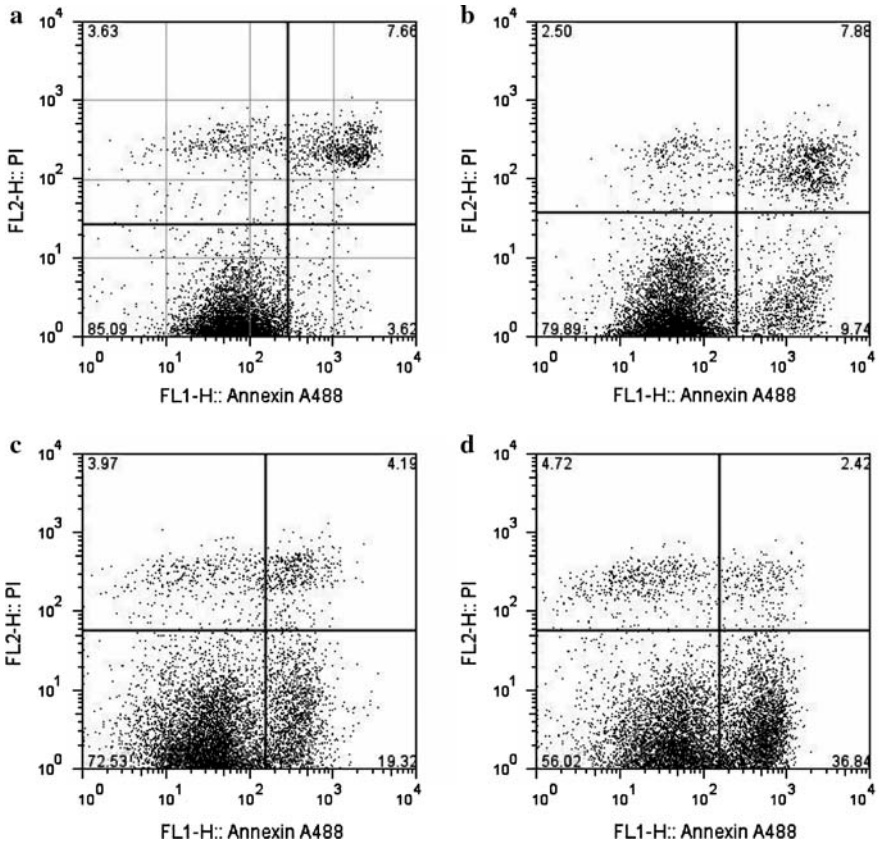

Fig. 7 Apoptosis following treatment with small Mn_3O_4 NP's. Lower left quadrant represents living cells, upper left quadrant dead cells and lower and upper right quadrants early and late apoptotic cells, respectively. The numbers denote the percent of cells in each quadrant. The NP concentrations were **a** nontreated, **b** 2.5, **c** 5, and **d** 10 μg/mL

present only in the cytoplasm and not to penetrate the nucleus.

The formation of ROS followed a different pattern than that observed for cytotoxicity. The ROS formation was greatest in cells exposed to K_xMnO_2 and decreased further in the following order MnOOH $\approx$ Mn_3O_4 > medium NP > large NP. Concentration dependence was observed for all nanomaterials, but was strongest for K_xMnO_2 and weakest for medium and large NP's. Both the ROS formation and cytotoxicity clearly indicate a size-dependent effect for the Mn_3O_4 NP's that corresponds to specific surface area. However, the lesser cytotoxicity and higher ROS formation observed with MnOOH and K_xMnO_2 (both of which have higher specific surface areas than the small Mn_3O_4) clearly indicate that other properties of the Mn oxides are more important than the specific surface area.

Activation of the transcription factor NF-κB (which has been related to oxidative stress) and the extent of cell apoptosis were examined for cells exposed to small Mn_3O_4 NP's. In both cases, concentration-dependent effects were observed, but further mechanistic studies are necessary in order to establish the mechanisms leading to cell death.

Acknowledgments We thank Dr Mark Davis for his support related to the equipment needed for the synthesis of the nanomaterials, Pat Koen and Jean Edens for their help with the electron microscopy experiments, and Rochelle Diamond for the help provided with flow cytometry. The funding for this project was provided by the Camille and Henry Dreyfus Foundation and the Davidow Innovative Environmental Research Fund.

References

Böttcher T, Mix E, Koczan D, Bauer P, Pahnke J, Peters S, Weinelt S, Knoblich R, Strauss U, Cattaneo E, Thiesen H-J (2003) Gene expression profiling of ciliary neurotrophic factor-overexpressing rat striatal progenitor cells (ST14A) indicates improved stress response during the early stage of differentiation. J Neurosci Res 73(1):42–53. doi:10.1002/jnr.10624

Braydich-Stolle L, Hussain S, Schlager JJ, Hofmann M-C (2005) In vitro cytotoxicity of nanoparticles in mammalian

germline stem cells. Toxicol Sci 88(2):412–419. doi:10.1093/toxsci/kfi256

Brenneman KA, Wong BA, Buccellato MA, Costa ER, Gross EA, Dorman DC (2000) Direct olfactory transport of inhaled manganese ($^{54}MnCl_2$) to the rat brain: toxicokinetic investigations in a unilateral nasal occlusion model. Toxicol Appl Pharmacol 169:238–248. doi:10.1006/taap.2000.9073

Brunner TJ, Wick P, Manser P, Spohn P, Grass RN, Limbach LK, Bruinink A, Stark WJ (2006) In vitro cytotoxicity of oxide nanoparticles: comparison to asbestos, silica, and the effect of particle solubility. Environ Sci Technol 40(14):4374–4381. doi:10.1021/es052069i

Chang E, Thekkek N, Yu WW, Colvin VL, Drezek R (2006) Evaluation of quantum dot cytotoxicity based on intracellular uptake. Small 2(12):1412–1417. doi:10.1002/smll.200600218

Chatterjee J, Haik Y, Chen C (2001) Synthesis and characterization of heat-stabilized albumin magnetic microspheres. Colloid Polym Sci 279(11):1073–1081. doi:10.1007/s003960100523

Chithrani BD, Chan WCW (2007) Elucidating the mechanism of cellular uptake and removal of protein-coated gold nanoparticles of different sizes and shapes. Nano Lett 7(6):1542–1550. doi:10.1021/nl070363y

Churg A (2003) Interactions of exogenous or evoked agents and particles: the role of reactive oxygen species. Free Radic Biol Med 34(10):1230–1235. doi:10.1016/S0891-5849(03)00175-8

Cohen DD, Gulson BL, Davis JM, Stelcer E, Garton D, Hawas O, Taylor A (2005) Fine-particle Mn and other metals linked to the introduction of MMT into gasoline in Sydney, Australia: results of a natural experiment. Atmos Environ 39:6885–6896. doi:10.1016/j.atmosenv.2005.08.006

Colvin VL (2003) The potential environmental impact of engineered nanomaterials. Nat Biotechnol 21(10):1166–1170. doi:10.1038/nbt875

Dobson AW, Erikson KM, Aschner M (2004) Manganese neurotoxicity. Redox-active metals in neurological disorders, Annals of the New York Academy of Sciences, vol 2012. New York Academy of Science, pp 115–128

Dorman DC, Struve MF, James RA, Marshall MW, Parkinson CU, Wong BA (2001) Influence of particle solubility on the delivery of inhaled manganese to the rat brain: manganese sulfate and manganese tetroxide pharmacokinetics following repeated (14-day) exposure. Toxicol Appl Pharmacol 170:79–87. doi:10.1006/taap.2000.9088

Elder A, Gelein R, Silva V, Feikert T, Opanashuk L, Carter J, Potter R, Maynard A, Ito Y, Finkelstein J et al (2006) Translocation of inhaled ultrafine manganese oxide particles to the central nervous system. Environ Health Perspect 114(8):1172–1178

Fechter LD, Johnson DL, Lynch RA (2002) The relationship of particle size to olfactory nerve uptake of a non-soluble form of manganese into brain. Neurotoxicology 23:177–183. doi:10.1016/S0161-813X(02)00013-X

Filipov NM, Seegal RF, Lawrence DA (2005) Manganese potentiates in vitro production of proinflammatory cytokines and nitric oxide by microglia through a nuclear factor kappa B-dependent mechanism. Toxicol Sci 84(1):139–148. doi:10.1093/toxsci/kfi055

Goodman CM, McCusker CD, Yilmaz T, Rotello VM (2004) Toxicity of gold nanoparticles functionalized with cationic and anionic side chains. Bioconjug Chem 15:897–900. doi:10.1021/bc049951i

Gulson B, Mizon K, Taylor A, Korsch M, Stauber J, Davis JM, Louie H, Wu M, Swan H (2006) Changes in manganese and lead in the environment and young children associated with the introduction of methylcyclopentadienyl manganese tricarbonyl in gasoline—preliminary results. Environ Res 100(1):100–114. doi:10.1016/j.envres.2005.03.013

Hiura TS, Kaszubowski MP, Li N, Nel AE (1999) Chemicals in diesel exhaust particles generate reactive oxygen radicals and induce apoptosis in macrophages. J Immunol 163(10):5582–5591

Hiura TS, Li N, Kaplan R, Horwitz M, Seagrave J-C, Nel AE (2000) The role of a mitochondrial pathway in the induction of apoptosis by chemicals extracted from diesel exhaust particles. J Immunol 165:2703–2711

Hussain SM, Hess KL, Gearhart JM, Geiss KT, Schlager JJ (2005) In vitro toxicity of nanoparticles in BRL 3A rat liver cells. Toxicol In Vitro 19(7):975–983. doi:10.1016/j.tiv.2005.06.034

Kreyling WG, Semmler-Behnke M, Moeller W (2006) Health implications of nanoparticles. J Nanopart Res 8:543–562. doi:10.1007/s11051-005-9068-z

Kumagai Y, Koide S, Taguchi K, Endo A, Nakai Y, Yoshikawa T, Shimojo N (2002) Oxidation of proximal protein sulfhydryls by phenanthraquinone, a component of diesel exhaust particles. Chem Res Toxicol 15(4):483–489. doi:10.1021/tx0100993

Li N, Venkatesan MI, Miguel A, Kaplan R, Gujuluva C, Alam J, Nel A (2000) Induction of heme oxygenase-1 expression in macrophages by diesel exhaust particle chemicals and quinones via the antioxidant-responsive element. J Immunol 165(6):3393–3401

Li N, Sioutas C, Cho A, Schmitz D, Misra C, Sempf J, Wang M, Oberley T, Froines J, Nel A (2003) Ultrafine particulate pollutants induce oxidative stress and mitochondrial damage. Environ Health Perspect 111(4):455–460

Limbach LK, Wick P, Manser P, Grass RN, Bruinink A, Stark WJ (2007) Exposure of engineered nanoparticles to human lung epithelial cells: influence of chemical composition and catalytic activity on oxidative stress. Environ Sci Technol 41(11):4158–4163. doi:10.1021/es062629t

Long TC, Saleh N, Tilton RD, Lowry GV, Veronesi B (2006) Titanium dioxide (P25) produces reactive oxygen species in immortalized brain microglia (BV2): Implications for nanoparticle neurotoxicity. Environ Sci Technol 40(14):4346–4352. doi:10.1021/es060589n

Manna SK, Sarkar S, Barr J, Wise K, Barrera EV, Jejelowo O, Rice-Ficht AC, Ramesh GT (2005) Single-walled carbon nanotube induces oxidative stress and activates nuclear transcription factor-kB in human keratinocytes. Nano Lett 5:1676–1684. doi:10.1021/nl0507966

Morgan JJ (2000) Manganese in natural waters and earth's crust: its availability to organisms. In: Sigel A, Sigel H (eds) Metal ions in biological systems. Marcel Dekker, New York, pp 1–34

Nel A, Xia T, Maedler L, Li N, Geffen D (2006) Toxic potential of materials at the nanolevel. Science 311:622–627. doi:10.1126/science.1114397

Oberdorster G (2001) Pulmonary effects of inhaled ultrafine particles. Int Arch Occup Environ Health 74:1–8. doi:10.1007/s004200000185

Oberdorster G, Oberdorster E, Oberdorster J (2005) Nanotoxicology: an emerging discipline evolving from studies of ultrafine particles. Environ Health Perspect 113(7):823–839

Pahl HL (1999) Activators and target genes of Rel/NF-kB transcription factors. Oncogene 18:6853–6866. doi:10.1038/sj.onc.1203239

Pan Y, Neuss S, Leifert A, Fischler M, Wen F, Simon U, Schmid G, Brandau W, Jahnen-Dechent W (2007) Size-dependent cytotoxicity of gold nanoparticles. Small 3(11):1941–1949. doi:10.1002/smll.200700378

Peters K, Unger RE, Kirkpatrick CJ, Gatti AM, Monari E (2004) Effects of nano-scaled particles on endothelial cell function in vitro: studies on viability, proliferation and inflammation. J Mater Sci Mater Med 15(4):321–325. doi:10.1023/B:JMSM.0000021095.36878.1b

Phillips DM (1998) Electron microscopy: use of transmission electron microscopy to study cells in culture. Methods Cell Biol 57:297–311. doi:10.1016/S0091-679X(08)61587-3

Rahman Q, Lohani M, Dopp E, Pemsel H, Jonas L, Weiss DG, Schiffmann D (2002) Evidence that ultrafine titanium dioxide induces micronuclei and apoptosis in Syrian hamster embryo fibroblasts. Environ Health Perspect 110(8):797–800

Rao DB, Wong BA, McManus BE, McElveen AM, James AR, Dorman DC (2003) Inhaled iron, unlike manganese, is not transported to the rat brain via the olfactory pathway. Toxicol Appl Pharmacol 193:116–126. doi:10.1016/S0041-008X(03)00340-5

Sakon S, Xue X, Takekawa M, Sasazuki T, Okazaki T, Kojima Y, Piao J-H, Yagita H, Okumura K, Doi T, Nakano H (2003) NF-kB inhibits TNF-induced accumulation of ROS that mediate prolonged MAPK activation and necrotic cell death. EMBO J 22:3898–3909. doi:10.1093/emboj/cdg379

Takizawa H, Ohtoshi T, Kawasaki S, Kohyama T, Desaki M, Kasama T, Kobayashi K, Nakahara K, Yamamoto K, Matsushima K, Kudoh S (1999) Diesel exhaust particles induce NF-kB activation in human bronchial epithelial cells in vitro: importance in cytokine transcription. J Immunol 162:4705–4711

Tjalve H, Henriksson J (1999) Uptake of metals in the brain via olfactory pathways. Neurotoxicology 20(2–3):181–196

Vitarella D, Wong BA, Moss OR, Dorman DC (2000) Pharmacokinetics of inhaled manganese phosphate in male Sprague–Dawley rats following subacute (14-day) exposure. Toxicol Appl Pharmacol 163:279–285. doi:10.1006/taap.1999.8874

Xia T, Kovochich M, Brant J, Hotze M, Sempf J, Oberley T, Sioutas C, Yeh JI, Wiesner MR, Nel AE (2006) Comparison of the abilities of ambient and manufactured nanoparticles to induce cellular toxicity according to an oxidative stress paradigm. Nano Lett 6(8):1794–1807. doi:10.1021/nl061025k

Zhang W, Wang C, Zhang X, Xie Y, Qian Y (1999) Low temperature synthesis of nanocrystalline Mn_3O_4 by a solvothermal method. Solid State Ion 117:331–335. doi:10.1016/S0167-2738(98)00432-9

Zhang W, Yang Z, Liu Y, Tang S, Han X, Chen M (2004) Controlled synthesis of Mn_3O_4 nanocrystallites and MnOOH nanorods by a solvothermal method. J Cryst Growth 263:394–399. doi:10.1016/j.jcrysgro.2003.11.099

Zhao HS, He W, Wang YJ, Yue YZ, Gao XG, Li ZM, Yan SP, Zhou WJ, Zhang XD (2008) Biomineralizing synthesis of mesoporous hydroxyapatite-calcium pyrophosphate polycrystal using ovalbumin as biosurfactant. Mater Chem Phys 111(2–3):265–270. doi:10.1016/j.matchemphys.2008.04.002